Electron Spin Resonance spectroscopy with femtoliter detection volume

V. Ranjan,[1] S. Probst,[1] B. Albanese,[1] T. Schenkel,[2] D. Vion,[1] D. Esteve,[1] J. J. L. Morton,[3] and P. Bertet[1, a)]
[1)] *Quantronics group, SPEC, CEA, CNRS, Université Paris-Saclay, CEA Saclay 91191 Gif-sur-Yvette Cedex, France*
[2)] *Accelerator Technology and Applied Physics Division, Lawrence Berkeley National Laboratory, Berkeley, California 94720, USA*
[3)] *London Centre for Nanotechnology, University College London, London WC1H 0AH, United Kingdom*

(Dated: 11 February 2020)

We report electron spin resonance measurements of donors in silicon at millikelvin temperatures using a superconducting LC planar micro-resonator and a Josephson Parametric Amplifier. The resonator includes a nanowire inductor, defining a femtoliter detection volume. Due to strain in the substrate, the donor resonance lines are heavily broadened. Single-spin to photon coupling strengths up to ~ 3 kHz are observed. The single shot sensitivity is 120 ± 24 spins/Hahn echo, corresponding to $\approx 12 \pm 3$ spins/$\sqrt{\text{Hz}}$ for repeated acquisition.

PACS numbers: 07.57.Pt,76.30.-v,85.25.-j

Electron spin resonance (ESR) spectroscopy is useful for characterizing paramagnetic species and finds applications in a large number of fields. The most widely used detection method is the so-called inductive detection, which relies on the emission of microwave signals by the spins during their Larmor precession into a resonant cavity to which they are magnetically coupled. Conventional inductively-detected ESR spectroscopy suffers from a low spin detection sensitivity, which precludes its use for micron- or nano-scale samples[1], motivating research on alternative detection schemes[2–9].

Planar micro-resonators[10,11] and self-resonant microhelices[12] have been shown to be promising to push inductive detection to higher sensitivity and lower detection volumes, but the microwave confinement that they enable is ultimately limited by ohmic losses in the metal. This can be overcome by the use of superconducting micro-resonators at low temperatures[13–16], for which arbitrarily small detection volumes should in principle be achievable while preserving a high resonator quality factor. An additional benefit of using small-mode-volume and high-quality-factor resonators is the enhanced microwave spontaneous emission they cause via the Purcell effect[16–19], which enables to repeat measurements faster and therefore impacts favorably the spin detection sensitivity. A recent experiment detected the ESR signal from an ensemble of donors in silicon at millikelvin temperatures coupled to a superconducting resonator with a sub-pL magnetic mode volume, reaching a spin detection sensitivity of 65 spin/$\sqrt{\text{Hz}}$ measured by a Hahn-echo sequence[20].

Here, we push this effort further with a new resonator geometry incorporating a superconducting nanowire around which the magnetic component of the microwave field is confined, yielding a mode volume as low as ~ 6 fL. Correspondingly, the spin-photon coupling constant reaches values up to 3 kHz, an order-of-magnitude enhancement over the state-of-the-art. We estimate a spin detection sensitivity of 12 ± 3 spins/$\sqrt{\text{Hz}}$ for donors in silicon at millikelvin temperatures. As a counterpart, the Rabi frequency is highly inhomogeneous. Also, due to differential thermal contractions between the substrate and the nanowire, the donor resonance is considerably broadened by strain.

An overview of our resonator design is shown in Fig. 1(b). The resonator is patterned out of a 50 nm-thick superconducting aluminum film. It consists of an interdigitated capacitor C with fingers 10 μm wide and separated by the same amount. The bowtie shape is chosen to minimize the stray inductance of this capacitor[16]. The resulting resonator impedance is estimated from electromagnetic simulations[21] to be $Z_c \sim 15\ \Omega$. The capacitor is shorted by a 100 nm-wide, 10 μm-long wire that constitutes the resonator inductance L, and around which the magnetic component of the microwave field is by far the strongest.

The resonator is patterned on top of a silicon substrate in which bismuth atoms were implanted between 50 and 100 nm below the surface (see Fig. 1). To increase the donor coherence time, the substrate was enriched in the nuclear-spin-free ^{28}Si isotope, with a nominal residual ^{29}Si relative concentration of 5×10^{-4}. Bismuth is an electron donor in silicon, and can trap the unpaired electron at low temperatures, whose electron spin $S = 1/2$ provides the ESR signal[22]. The donor spin Hamiltonian is $H/\hbar = \gamma_e \mathbf{S} \cdot \mathbf{B_0} + A\mathbf{S} \cdot \mathbf{I}$, where $I = 9/2$ is the nuclear spin of the bismuth ion, $A/2\pi = 1.45$ GHz the hyperfine coupling, and B_0 the value of a dc magnetic field applied parallel to the nanowire inductor (along the z axis). At low magnetic fields B_0, the ESR-allowed transitions[23–26] are shown in Fig. 2(a). Note the zero-field splitting of 7.38 GHz enabling measurements at low fields (< 10 mT in this work).

A schematic description of the setup is shown in Fig. 1(a). The sample is cooled at 20 mK, and probed by microwave reflectometry. Sequences of microwave pulses at the resonator frequency are applied to the sample in-

[a)] patrice.bertet@cea.fr

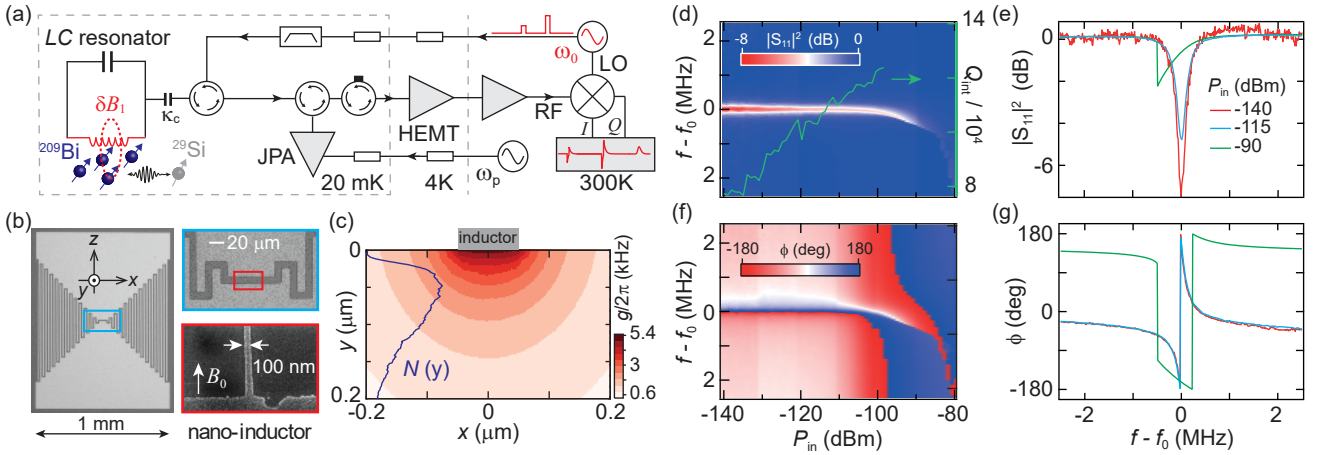

FIG. 1. Quantum limited spectrometer. (a) Schematics of the measurement setup. Square control pulses are applied at resonator frequency ω_0. Reflected and emitted signals from spins are amplified by a JPA in its degenerate mode, i.e. when pumped at $\omega_p \approx 2\omega_0$. (b) Optical and scanning electron microscope images of the LC resonator with a nanometric inductor. Light and dark areas form the aluminium and the underlying Si substrate, respectively. The magnetic field is applied parallel to the inductor. (c) Calculated spin-resonator coupling strength distribution for the first spin-transition. Implantation profile $N(y)$ with peak concentration of 8×10^{16} cm^{-3} is also plotted. Reflected power (d,e) and phase (f,g) from continuous wave measurements for resonator S1 at different input powers $P_{\rm in}$. Extracted internal quality factor $Q_{\rm int}$ is plotted on the right axis of panel (d).

put to drive the spins. The reflected pulses and emitted echo-signals are routed via a cryogenic circulator to the detection chain, consisting of a Josephson Parametric Amplifier (JPA)[27] at 20 mK followed by a High-Electron-Mobility Transistor (HEMT) at the 4K stage. The signal quadratures are then obtained by homodyne demodulation at room temperature. A phase cycling scheme is applied: we subtract two consecutive traces with the first pulse phase being changed from $+\pi/2$ to $-\pi/2$, which minimizes the impact of setup drifts. More details can be found in Ref. 15 and 20. Results from two nearly identical samples (S1 and S2) are reported below; unless mentioned explicitly, measurements reported have been performed on sample S1.

The resonator parameters are first determined by measuring its complex reflection coefficient S_{11} with a vector network anlyzer (VNA); it is shown for S1 in Fig. 1(d,f), as a function of the input power. At the lowest power ($P_{\rm in} = -140$ dBm), the resonance is well fitted by a Lorentzian, yielding a frequency $\omega_0/2\pi = 7.25$ GHz, an external quality factor $Q_{\rm ext} = 3 \times 10^4$, and an internal quality factor $Q_{\rm int} = 8 \times 10^4$. At larger power, the internal quality factor is observed to progressively increase, up to $Q_{\rm int} = 1.2 \times 10^5$ for $P_{\rm in} = -100$ dBm. Such power-dependent internal losses are characteristic of dielectric losses caused by two-level systems and are commonly observed in superconducting micro-resonators[28]. From ~ -100 dBm to ~ -90 dBm, the resonance appears to shift to lower frequencies, and its response in amplitude deviates progressively from a Lorentzian; at powers above -90 dBm it shows abrupt changes as seen in Fig. 1(e,g). Similar results are obtained for sample S2, with a frequency of 7.56 GHz and a total quality factor of 6×10^3 dominated by external coupling. Such behavior is characteristic of the Kerr non-linearity caused by the nanowire kinetic inductance (which can be harnessed to achieve parametric amplification of microwave signals[29]). For pulsed ESR spectroscopy, microwave pulses at ω_0 are applied to drive the spins. Given the resonator non-linearity, it is preferable to use drive pulses with maximum input power lower than -100 dBm. With a slightly larger input power (between ~ -100 dBm and ~ -90 dBm), the intra-cavity field acquires a deterministic time-dependent phase shift, which causes the resulting echo signal to be non-trivially distributed on both the in-phase and out-of-phase quadratures; the echo magnitude itself is however little affected and this weakly non-linear regime can thus also be used for pulse ESR spectroscopy[30].

An important parameter is the spin-photon coupling strength $g_0 = \gamma_e \langle 0|S_x|1\rangle \delta B_1$, defined as half the Rabi frequency that a spin would undergo in δB_1, the microwave amplitude corresponding to a 1 photon field, $\gamma_e/2\pi = 28$ GHz/T being the free electron gyromagnetic ratio and $\langle 0|S_x|1\rangle$ the spin transition matrix element between the two levels $|0\rangle$ and $|1\rangle$ whose frequency difference is equal to ω_0 at the applied B_0. The spin-photon coupling strength for the lowest-frequency bismuth donor transition is shown in Fig. 1(c). The magnetic field δB_1 was calculated using an electromagnetic solver assuming that the ac current corresponding to 1 photon in the resonator $\delta i = \omega_0 \sqrt{\hbar/2Z_c}$ flows through the inductor. Close to the nanowire within a depth of 40 nm, $g_0/2\pi$ reaches values as high as 3 − 5 kHz, one order of magnitude larger

than spin-resonator couplings measured so far[20], thanks to the extreme confinement of the microwave field around the nanowire. The price to pay however is a large spatial inhomogeneity of g_0. Consequences of a wide distribution of g_0 values when combined with spin relaxation by the Purcell effect were analyzed in Ref. 31 for typical pulse ESR sequences. Consider a two-pulse-echo sequence, consisting of a first microwave pulse of amplitude $\beta/2$ and duration dt, followed by a waiting time τ, and by a second pulse of amplitude β and duration dt [see Fig. 2(a)] with $\beta = \sqrt{P_{\rm in}/\hbar\omega_0}$ (β^2 represents number of incoming photons per second). Because of the g_0 inhomogeneous distribution, the spin echo signal observed a time τ after the second pulse receives its dominant contribution from spins with a coupling constant $g_0(\beta) = \pi\sqrt{\kappa}/(4\beta dt)$, because those undergo Rabi angles close to $\pi/2$ and π. It is therefore possible to probe spins with different coupling constants by changing the amplitude β of the detection echo sequence[31].

A first example of this selectivity is provided by spectrum measurements shown in Fig. 2(a). The integral A_e of a spin-echo is displayed as a function of the value of the magnetic field B_0, applied parallel to the inductor. Two spectra measured in S2 are displayed, for two values of β (corresponding to input powers of -100 dBm and -86 dBm). In the high-power spectrum, two narrow peaks (solid line) are observed close to the expected bismuth donor ESR transitions, on top of an approximately constant signal that extends until $B_0 = 0$. In the low-power spectrum, the peaks vanish and only the nearly constant echo signal is observed. Only the low-power curve was measured with resonator S1, and a spectrum similar to the one of sample S2 is observed [see Fig. 2(a)].

These observations suggest that bismuth donors spins closest to the wire (those detected in the low-power measurement) have a very broad spectrum, whereas those far from the wire (detected in the high-power measurement) have narrower linewidth. This can be qualitatively understood by the effect of mechanical strain on the spin properties of bismuth donors. The hyperfine constant was recently shown[32] to depend linearly on the hydrostatic strain ϵ, with $(dA/d\epsilon)/2\pi \sim 29$ GHz. Aluminum contracts 10 times more than silicon upon cooldown from room-temperature to 10 mK. The calculated strain profile ϵ in the silicon resulting from the differential thermal contraction of the aluminum inductor patterned on top is shown in Fig. 2(b)[33]. For spins located in the region close to the inductance (and therefore strongly coupled to the resonator), the standard-deviation in the zero-field splitting (equal to $5A/2\pi$) is ~ 100 MHz, which is sufficient to account for a complete overlap of neighboring peaks and therefore a nearly flat spectrum. Spins further from the inductor are submitted to much lower strain, leading to better-resolved transitions.

One consequence of this broadening for donors near the inductor is that each of the 10 Bismuth transitions may contribute to the spin-echo signal measured at a given B_0, as schematically explained in Fig. 2(a). We take

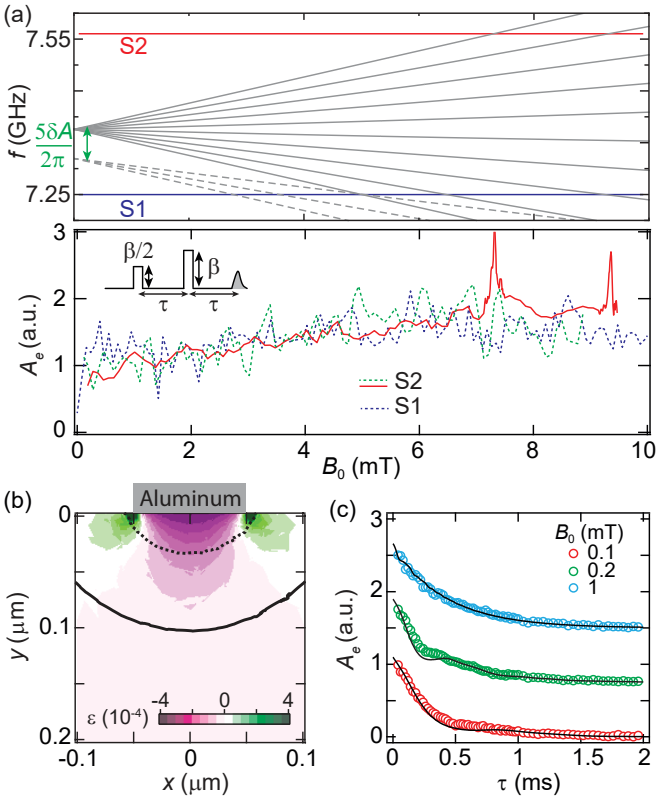

FIG. 2. Spin spectroscopy (a) Top: Ten electron spin transitions of bismuth in the low magnetic field regime. The dashed lines represent new frequencies for first three transitions due to changes in hyperfine constant δA by local strain. Bottom: Magnetic field sweep of the echo signal for two devices fabricated on the same substrate (sequence in inset). Different curves are scaled in amplitude and acquired at different pulse amplitudes β. For device S2, $\beta = 2\times10^5$ s$^{-1/2}$ (dashed curve), 7×10^5 s$^{-1/2}$ and the pulse duration $dt = 0.5$ μs. For device S1, $\beta = 10^5$ s$^{-1/2}$ and $dt = 1$ μs. (b) Hydrostatic component ϵ of the strain computed using finite element model simulations of COMSOL software. Solid and dashed curves represent respective contours of probed spins in S2 when assuming perfect π pulses for two β values. (c) Two pulse spin coherence measurements with S1: Echo area A_s as a function of delay τ. Curves have been offset for clarity. Solid curves are simulations.

that into account in our analysis as explained below.

To examine that the echo signals arise from implanted bismuth donors and not from surface impurities, we get information about the electron spin environment using hyperfine spectroscopy. The integrated spin-echo amplitude A_e is measured as a function of τ for various values of B_0 [see Fig. 2(c)]. For $B_0 \geq 1$ mT, the decay is exponential, with a decay constant $T_2 = 0.85 \pm 0.1$ ms, a coherence time somewhat shorter than comparable measurements in identical silicon samples in refs.[15,20]. At $B_0 < 1$ mT, slight oscillations are visible. They approximately match the expected Electron Spin Echo Envelope Modulation (ESEEM) by a bath of ^{29}Si nuclei with the nominal relative concentration of 5×10^{-4} [see Fig. 2(c)]

[34]. This suggests that the spin-echo signals result from spins located in the bulk of the silicon sample.

In the Purcell regime, $T_1 = \kappa/(4g_0^2)$ at resonance, implying that the spin-photon coupling constant can be deduced from spin relaxation measurements. The corresponding spin relaxation sequence (saturation recovery) consists of a long saturation pulse, followed after a delay T by a detection-echo whose pulse amplitude $\beta_0 = 6 \times 10^4$ s$^{-1/2}$ ($P_{\rm in} \approx -107$ dBm, thus in the resonator linear regime) mostly selects a class of spins with coupling constant $g_0(\beta_0)$. The integrated echo is shown in Fig. 3(a) as a function of T. An exponential fit yields $T_1 = 2 \pm 0.4$ ms, which translates into a coupling constant $g_0(\beta_0)/2\pi = 2.7$ kHz. This is the largest spin-photon magnetic coupling measured, confirming the predicted coupling distribution [Fig. 1(c)]. Larger values may be obtained using superconducting flux-qubits[35]. As discussed in Ref. 31, the measured relaxation time scales as β^2, in good agreement with simulations. This enables us to calibrate β in absolute units, which is otherwise difficult because of the imperfect knowledge of the total attenuation in the input line. The validity of the calibration is confirmed by a Rabi nutation experiment, measured with a pulse sequence shown in Fig. 3(b). The integrated echo area is shown as a function of the amplitude $\beta_{\rm inv}$ of a first microwave pulse, followed by a detection echo. The simulation agrees quantitatively with the data, without adjustable parameter.

We then estimate the spectrometer sensitivity following the method explained in Ref. 20. The number of spins $N_{\rm spin}$ contributing to an echo signal, defined as the total number of spins excited after the initial pulse is first determined: we measure a complete Hahn-echo sequence, including two control pulses of amplitude $\beta_0/2, \beta_0$ and duration 1 μs separated by 50 μs. The JPA was switched off to avoid its saturation during application of the control pulses. The reflected amplitude, obtained after 10^6 averages measured with a repetition rate of 100 Hz, is shown in Fig. 3(c). Since the ratio between echo and control pulse amplitude is uniquely determined by $N_{\rm spin}$, the latter is obtained by adjusting the simulations to best fit the data [see solid line in Fig. 3(c)], yielding $N_{\rm spin} \approx 36 \pm 8$. We note that all ten transitions are equally weighted to account for the overlap of the ESR transition due to strain-induced large spectral broadening. This number is also roughly consistent with the number of bismuth atoms expected in the resonator magnetic mode volume, taking into account that the spin resonance linewidth is considerably broader than the detection bandwidth.

The signal-to-noise ratio (SNR) is measured by acquiring 10^4 echo traces (with phase cycling) in the degenerate mode of the JPA at $\gamma_{\rm rep} = 100$ Hz. From the histogram shown in Fig. 3(d), we find that the SNR is 0.33 for a single echo trace. Therefore, one could detect $N_{\rm min} \approx 120 \pm 24$ spins with unity SNR in a single echo sequence. Since the measurements are repeated with 100 Hz repetition rate, this translates into a spin detection sensitivity of 12 ± 3 spins/$\sqrt{\rm Hz}$. Theoretical estimates of the sensitivity[15] predict that $N_{\rm min} = \frac{\kappa}{2Pg_0}\sqrt{\tilde{n}}$, $\tilde{n} = 1/2$ being the noise due to quantum fluctuations of the microwave field and $P \approx 1$, the thermal polarization of the spins at 20 mK. For $g_0/2\pi = 2.7$ kHz, this yields $N_{\rm min} = 50$, in semi-quantitative agreement with the measured value. Further improvements in sensitivity would require to further increase g_0 or the quality factor, or to reduce the noise below the quantum limit using squeezed vacuum for instance, as demonstrated recently[36].

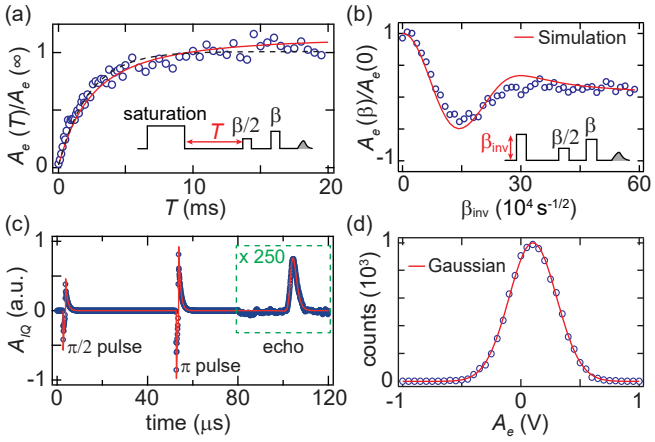

FIG. 3. Spectrometer sensitivity. (a) Spin relaxation time measured using the saturation recovery method. The dashed curve is the best fit to an exponential yielding $T_1 = 2 \pm 0.4$ ms. (b) Rabi oscillations performed using three pulse sequence shown in the inset at $\gamma_{\rm rep} = 50$ Hz. (c) Measurement of the reflected amplitude A_{IQ} showing a complete Hahn echo sequence. (d) Histograms of echoes at $\gamma_{\rm rep} = 100$ Hz measured with phase cycling. Solid curves in panels (a-c) are numerical simulations taking into account all ten ESR transitions.

Expressing the spin sensitivity in spin/$\sqrt{\rm Hz}$ assumes that repeating the same sequence n times and averaging the result increases the SNR by $\sqrt{n}$. We test this assumption by acquiring 10^7 echo sequences, repeated with a rate of 100 Hz, generating a histogram obtained by averaging n consecutive echo integrals, and computing the standard deviation $\sigma(n)$. The result is shown in Fig. 4(a). We observe that, while $\sigma(n)$ indeed scales like $1/\sqrt{n}$ until $n = 200$, it keeps going down for larger values of n but slower than $1/\sqrt{n}$.

To test whether the deviation of $\sigma(n)$ from $1/\sqrt{n}$ is due to the setup or to the sample, we mimic the echo acquisition by sending a train of weak coherent pulses with an amplitude that corresponds to an echo and the same repetition rate of 100 Hz at the resonator frequency ω_0. Their standard deviation now follows the $1/\sqrt{n}$ law until at least $n = 10^4$, implying that the slower-than-$\sqrt{n}$ echo averaging is not due to setup drift. Note that compared (and contrary) to the analysis performed in Ref. 20, the test pulses were sent at the resonator frequency ω_0 so that they would be affected by resonator phase noise, which can thus be ruled out as the origin of the slower-than-$\sqrt{n}$

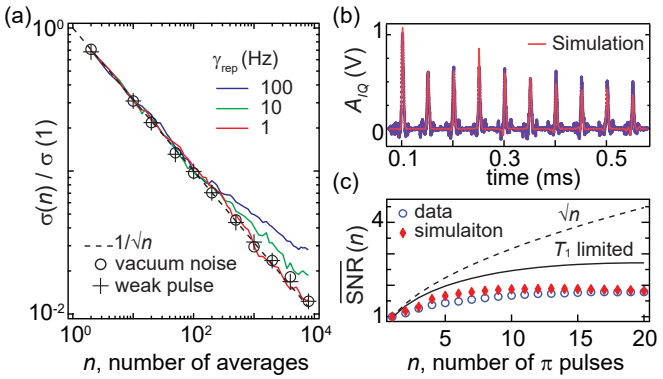

FIG. 4. Correlated noise and CPMG sequences (a) Measured standard deviation of signals versus number n of averages shown by solid lines and symbols. (b) In symbols, averaged amplitude of 10^4 repetitions of CPMG traces measured at $\gamma_{\rm rep} = 100$ Hz in the degenerate mode of the JPA. Refocusing pulses are not visible due to phase cycling. (c) Improvement of echo SNR with number of refocusing π pulses. Simulated SNR (diamond symbols), and calculated curves for cases of no energy relaxation (dashed line) and finite relaxation (solid line) assuming uncorrelated noise between echoes.

echo signal averaging.

Further insight is obtained by analysing the spin-echo data differently: instead of averaging n consecutive echo traces, we average them with a separation of 10, or 100 traces (which amounts to effectively changing the repetition rate to 10 Hz or 1 Hz). As seen in Fig. 4(a), the $1/\sqrt{n}$ law is progressively recovered. A possible interpretation is that the number of spins contributing to the echo slightly fluctuates over a time scale of a few seconds, possibly due to a slow redistribution of the bismuth donor population within the hyperfine states or to ionization/neutralization dynamics of one or a few donors located close to the metallic electrodes.

One way to increase the spectrometer SNR is to add extra refocusing pulses after the emission of the Hahn echo in order to obtain several echoes per sequence[15,37]. To this end, we use a Carr-Purcell-Meiboom-Gill (CPMG) sequence: $(\pi/2)_{\pm x} - \tau - \pi_y - \tau - (-echo - \tau/2 - \pi_y - \tau/2-)_n - echo$. The echo train generated by this sequence is shown as symbols in Fig. 4(b) for $\tau = 50$ μs (the refocusing pulses are not visible due to phase cycling). The numerical simulation plotted as a solid line describes well the change in the amplitude over time, without any adjustable parameter other than the overall amplitude. Note that the echo amplitude quickly decays after the first pulse, due to the large pulse errors caused by the B_1 inhomogeneity. In order to quantify the SNR improvement, we measure 10^4 sequences of CPMG echoes (with a repetition rate $\gamma_{\rm rep} = 100$ Hz). We then generate histograms obtained by averaging the first n echoes of each sequence, divide the mean by the standard deviation, yielding the SNR as a function of n. We find a maximum SNR improvement of ≈ 2, which corresponds to a spin detection sensitivity of 6 spins/$\sqrt{\rm Hz}$. This enhancement is well reproduced by simulations and is not far from the maximum limit ~ 2.7 set by the energy relaxation [see Fig. 4(c)].

In summary we demonstrate a sensitivity of 12 spins/$\sqrt{\rm Hz}$ in inductively-detected ESR spectroscopy, using a resonator based on a superconducting nanowire with a 6 fL detection volume. The spin-resonator coupling reaches values up to 3 kHz. An ESEEM signal originating from ~ 30 electron spins coupled to residual ^{29}Si nuclear spins was detected. Future work will study possible applications of superconducting ESR spectroscopy to real-world systems, for instance paramagnetic defects in two-dimensional Van der Waals materials[38].

We acknowledge technical support from P. Sénat and P.-F. Orfila, as well as stimulating discussions within the Quantronics group. We acknowledge support of the European Research Council under the European Community's Seventh Framework Programme (FP7/2007-2013) through grant agreements No. 615767 (CIRQUSS), 279781 (ASCENT), and 630070 (quRAM), of the ANR projects QIPSE and NASNIQ (contract number ANR-17-CHIN-0001). T. S. was supported by the U.S. Department of Energy under Contract No. DE-AC02-05CH11231.

[1] A. Schweiger and G. Jeschke, *Principles of pulse electron paramagnetic resonance* (Oxford University Press, 2001).
[2] J. Wrachtrup, C. Von Borczyskowski, J. Bernard, M. Orritt, and R. Brown, Nature **363**, 244 (1993).
[3] A. Gruber, A. Drbenstedt, C. Tietz, L. Fleury, J. Wrachtrup, and C. v. Borczyskowski, Science **276**, 2012 (1997).
[4] D. Rugar, C. Yannoni, and J. Sidles, Nature **360**, 563 (1992).
[5] D. Rugar, R. Budakian, H. Mamin, and B. Chui, Nature **430**, 329 (2004).
[6] R. V. Chamberlin, L. A. Moberly, and O. G. Symko, Journal of Low Temperature Physics **35**, 337 (1979).
[7] Y. Manassen, R. J. Hamers, J. E. Demuth, and A. J. Castellano Jr., Phys. Rev. Lett. **62**, 2531 (1989).
[8] S. Baumann, W. Paul, T. Choi, C. P. Lutz, A. Ardavan, and A. J. Heinrich, Science **350**, 417 (2015).
[9] A. Morello, J. J. Pla, F. A. Zwanenburg, K. W. Chan, K. Y. Tan, H. Huebl, M. Mottonen, C. D. Nugroho, C. Yang, J. A. van Donkelaar, and others, Nature **467**, 687 (2010).
[10] R. Narkowicz, D. Suter, and I. Niemeyer, Review of Scientific Instruments **79**, 084702 (2008).
[11] Y. Artzi, Y. Twig, and A. Blank, Applied Physics Letters **106**, 084104 (2015).
[12] J. W. Sidabras, J. Duan, M. Winkler, T. Happe, R. Hussein, A. Zouni, D. Suter, A. Schnegg, W. Lubitz, and E. J. Reijerse, Science Advances **5**, eaay1394 (2019).
[13] H. Malissa, D. I. Schuster, A. M. Tyryshkin, A. A. Houck, and S. A. Lyon, Review of Scientific Instruments **84**, 025116 (2013).
[14] A. J. Sigillito, H. Malissa, A. M. Tyryshkin, H. Riemann, N. V. Abrosimov, P. Becker, H.-J. Pohl, M. L. W. Thewalt, K. M. Itoh, J. J. L. Morton, A. A. Houck, D. I. Schuster, and S. A. Lyon, Applied Physics Letters **104**, (2014).
[15] A. Bienfait, J. Pla, Y. Kubo, M. Stern, X. Zhou, C.-C. Lo, C. Weis, T. Schenkel, M. Thewalt, D. Vion, D. Esteve, B. Julsgaard, K. Moelmer, J. Morton, and P. Bertet, Nature Nanotechnology **11**, 253 (2015).
[16] C. Eichler, A. J. Sigillito, S. A. Lyon, and J. R. Petta, Phys. Rev. Lett. **118**, 037701 (2017).
[17] E. M. Purcell, Phys. Rev. **69**, 681 (1946).

[18]P. Goy, J. M. Raimond, M. Gross, and S. Haroche, Physical Review Letters **50**, 1903 (1983).
[19]A. Bienfait, J. Pla, Y. Kubo, X. Zhou, M. Stern, C.-C. Lo, C. Weis, T. Schenkel, D. Vion, D. Esteve, J. Morton, and P. Bertet, Nature **531**, 74 (2016).
[20]S. Probst, A. Bienfait, P. Campagne-Ibarcq, J. J. Pla, B. Albanese, J. F. D. S. Barbosa, T. Schenkel, D. Vion, D. Esteve, K. Moelmer, J. J. L. Morton, R. Heeres, and P. Bertet, Applied Physics Letters **111**, 202604 (2017).
[21]CST Microwave Studios®.
[22]G. Feher, Phys. Rev. **114**, 1219 (1959).
[23]G. W. Morley, M. Warner, A. M. Stoneham, P. T. Greenland, J. van Tol, C. W. Kay, and G. Aeppli, Nature materials **9**, 725 (2010).
[24]M. H. Mohammady, G. W. Morley, and T. S. Monteiro, Physical Review Letters **105** (2010), 10.1103/physrevlett.105.067602.
[25]R. E. George, W. Witzel, H. Riemann, N. V. Abrosimov, N. Ntzel, M. L. W. Thewalt, and J. J. L. Morton, Physical Review Letters **105**, 067601 (2010).
[26]G. Wolfowicz, A. M. Tyryshkin, R. E. George, H. Riemann, N. V. Abrosimov, P. Becker, H.-J. Pohl, M. L. W. Thewalt, S. a. Lyon, and J. J. L. Morton, Nature Nanotechnology **8**, 561 (2013).
[27]X. Zhou, V. Schmitt, P. Bertet, D. Vion, W. Wustmann, V. Shumeiko, and D. Esteve, Phys. Rev. B **89**, 214517 (2014).
[28]J. M. Martinis, K. B. Cooper, R. McDermott, M. Steffen, M. Ansmann, K. D. Osborn, K. Cicak, S. Oh, D. P. Pappas, R. W. Simmonds, and C. C. Yu, Physical Review Letters **95**, 210503 (2005).
[29]E. M. Levenson-Falk, R. Vijay, and I. Siddiqi, Applied Physics Letters **98**, 123115 (2011).
[30]A. T. Asfaw, A. J. Sigillito, A. M. Tyryshkin, T. Schenkel, and S. A. Lyon, Applied Physics Letters **111**, 032601 (2017).
[31]V. Ranjan, S. Probst, B. Albanese, A. Doll, O. Jacquot, E. Flurin, R. Heeres, D. Vion, D. Esteve, J. J. L. Morton, and P. Bertet, Journal of Magnetic Resonance **310**, 106662 (2020).
[32]J. Mansir, P. Conti, Z. Zeng, J. Pla, P. Bertet, M. Swift, C. Van de Walle, M. Thewalt, B. Sklenard, Y. Niquet, and J. Morton, Physical Review Letters **120**, 167701 (2018).
[33]J. Pla, A. Bienfait, G. Pica, J. Mansir, F. Mohiyaddin, Z. Zeng, Y. Niquet, A. Morello, T. Schenkel, J. Morton, and P. Bertet, Physical Review Applied **9**, 044014 (2018).
[34]S. Probst, G. L. Zhang, M. Rancic, V. Ranjan, M. L. Dantec, Z. Zhong, B. Albanese, A. Doll, R. B. Liu, J. J. L. Morton, T. Chanelilere, P. Goldner, D. Vion, D. Esteve, and P. Bertet, arXiv:2001.04854 [quant-ph] (2020), arXiv: 2001.04854.
[35]X. Zhu, S. Saito, A. Kemp, K. Kakuyanagi, S.-i. Karimoto, H. Nakano, W. J. Munro, Y. Tokura, M. S. Everitt, K. Nemoto, M. Kasu, N. Mizuochi, and K. Semba, Nature **478**, 221 (2011).
[36]A. Bienfait, P. Campagne-Ibarcq, A. Kiilerich, X. Zhou, S. Probst, J. Pla, T. Schenkel, D. Vion, D. Esteve, J. Morton, K. Moelmer, and P. Bertet, Physical Review X **7**, 041011 (2017).
[37]F. Mentink-Vigier, A. Collauto, A. Feintuch, I. Kaminker, V. Tarle, and D. Goldfarb, Journal of Magnetic Resonance **236**, 117 (2013).
[38]A. K. Geim and I. V. Grigorieva, Nature **499**, 419 (2013).